SAND 78-0700
Unlimited Release

SENSITIVITY OF SLOPE MEASUREMENTS ON PARABOLIC SOLAR MIRRORS TO POSITIONING AND ALIGNMENT OF THE LASER SCANNER

L. Orear

Prepared by Sandia Laboratories, Albuquerque, New Mexico 87115
and Livermore, California 94550 for the United States Energy Research
and Development Administration under Contract AT (29-1)-789

May, 1978

Sandia Laboratories

Issued by Sandia Laboratories, operated for the United States Department of Energy by Sandia Corporation.

SF 1004-DF(11-77)

Printed in the United States of America
Available from
National Technical Information Service
U. S. Department of Commerce
5285 Port Royal Road
Springfield, VA 22151
Price: Printed Copy $5.00; Microfiche $2.25

TABLE OF CONTENTS

SAND 78-0700
Unlimited Release
April, 1978

SENSITIVITY OF SLOPE MEASUREMENTS ON PARABOLIC SOLAR MIRRORS TO POSITIONING AND ALIGNMENT OF THE LASER SCANNER*

L. Orear
Sandia Laboratories
Albuquerque, New Mexico 87185

ABSTRACT

A laser scanning system for measuring the geometric accuracy of parabolic solar concentrators in both laboratory and field situations is being developed at Sandia Laboratories. Inaccuracies in positioning and aligning this device with respect to the parabola reference system will introduce systematic errors in the measured data. The nature and sensitivity of these measurement errors are analyzed and evaluated by means of a mathematical model and computer simulation techniques. Distinctive patterns of apparent error in the collector surface geometry are introduced by inaccuracies in three apparatus set up parameters: vertical position, angular alignment, and horizontal position. These error patterns scale in proportion to the magnitude of the relevant set-up inaccuracy. Our studies allowed recognition of the subsequent compensation for the effects introduced by errors in the vertical position and the angular alignment. But, the similarity between patterns generated by errors in the horizontal position and those due to deviations in parabola focal length precluded the use of pattern recognition techniques. This ambiguity between error sources introduces an uncertainty in the best fit focal length estimated from scanning data which is equal to 0.42 times the uncertainty in horizontal positioning. In addition, the practical lower bounds for all three set-up

*This work supported by the United States Department of Energy.

tolerances are dependent on the resolution of the system detector. Analysis of worst case error combinations indicate the need for yet closer positioning and alignment tolerances.

INTRODUCTION

The optical efficiency of a concentrating solar mirror is governed by both geometrical accuracy and specular reflectance properties. A laser scanning system is under development at Sandia Laboratories which will measure the geometric accuracy of parabolic trough concentrators both in laboratory and field situations. In the early stages of this program it became apparent that errors in horizontal and vertical positioning together with angular misalignment with respect to the parabola reference system would introduce inaccuracies in the subsequent measurements.

In order to evaluate the nature and degree of measurement sensitivity to these set-up errors, a mathematical model has been developed. The model assumes the optimum scanning distance has been chosen for a parabolic trough of given focal length and rim-to-rim dimension, and that the mirror surface is theoretically perfect. Various set-up errors can therefore be systematically introduced and their resulting effects on measurement accuracy are simulated. From these simulation studies certain preliminary set-up and alignment tolerances are established.

In this paper the laser scanning system is first described and the set-up errors are identified. Next the mathematical model is developed and then the simulation procedure is explained. Finally the results of the sensitivity studies are presented and the implied set-up tolerances are discussed together with the limitations inherent in the geometric relationships of the scanning system.

DESCRIPTION

A radial scan laser inspection system for parabolic solar concentrators was conceived by B. L. Butler and D. W. Tipping of Sandia Laboratories.[1] This system, using a translating and rotating laser beam, is shown schematically in Figure 1 as it would be set up to inspect an East-West parabolic trough.[2]

In a typical measurement sequence, the system scans from rim to rim vertically, translates along the axis of the right parabolic cylinder, then scans rim to rim and so on until the translation carriage reaches the end of its four meter travel. The return beam intersects a detector which rotates with -- and is always assumed to be fixed perpendicular to -- the scanning ray. This return ray position is used to calculate the possible deviation of mirror surface slope from the ideal parabola slope at each sample point. Surface slope errors parallel to the trough length are not measured since they only divert collected light along the receiver tube rather than away from it. The ideal geometry for each rim-to-rim scan is shown in Figure 2. When accurately aligned the fixed laser beam directed perpendicular to the plane of the paper is reflected 90° by the rotating prism at point G. The scanning ray intersects the parabola at point P_i where it is reflected and intersects the detector at a distance d_i from the detector center. For a perfect parabola the position of the return ray is a function of the angle ϕ_i, the scanning distance r, and the parabola focal length f. The mechanical alignments which must be made to assure accurate parabola surface slope mapping entail positioning the carriage track parallel to the trough axis and aligning the rotating prism such that at 0° the beam passes through both the focus and vertex of the parabola.

Deviations of the return ray from its calculated position can be attributed to either (1) deviations of the parabola surface being measured from the desired

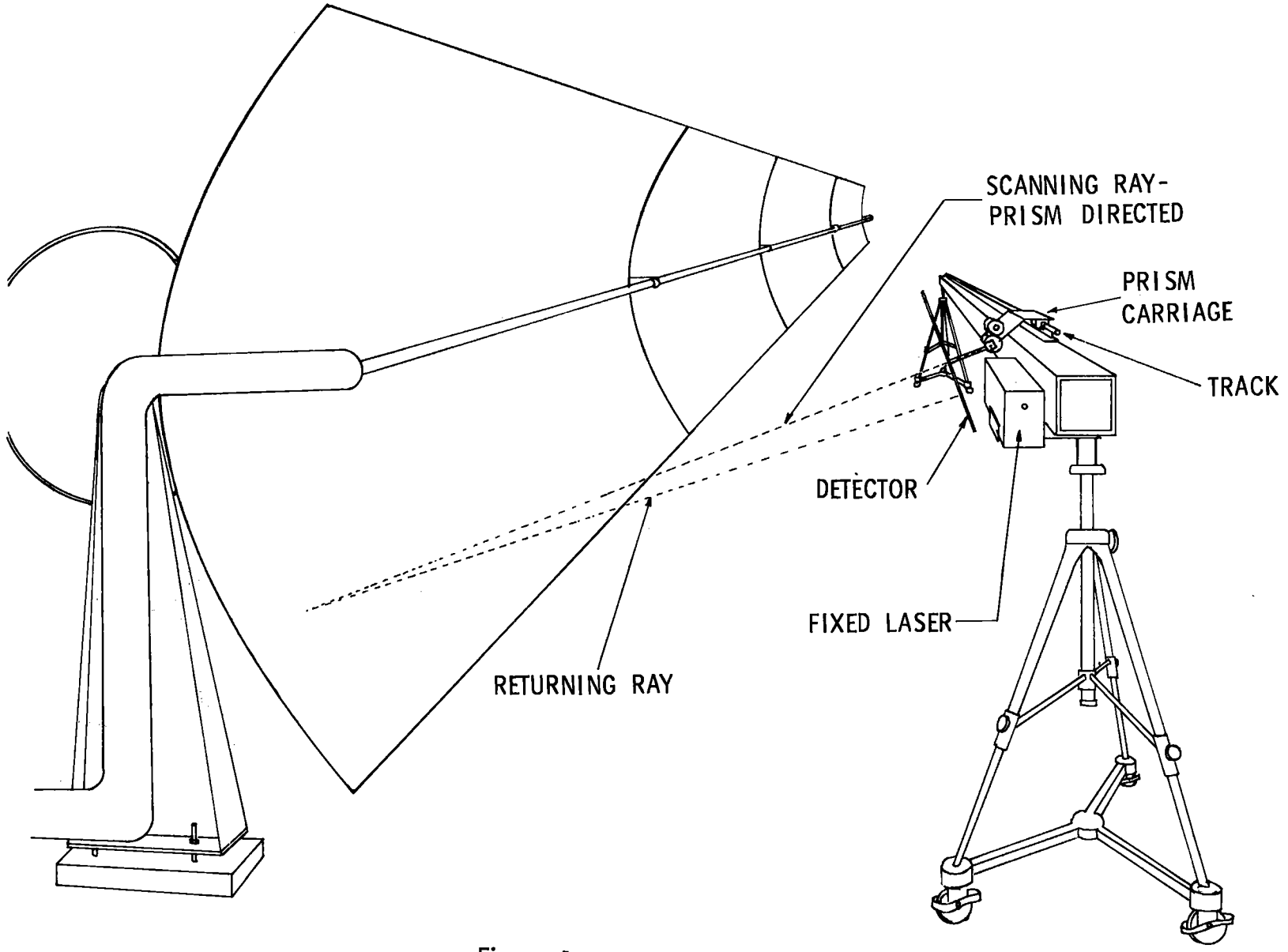

Figure 1. Laser Ray Trace

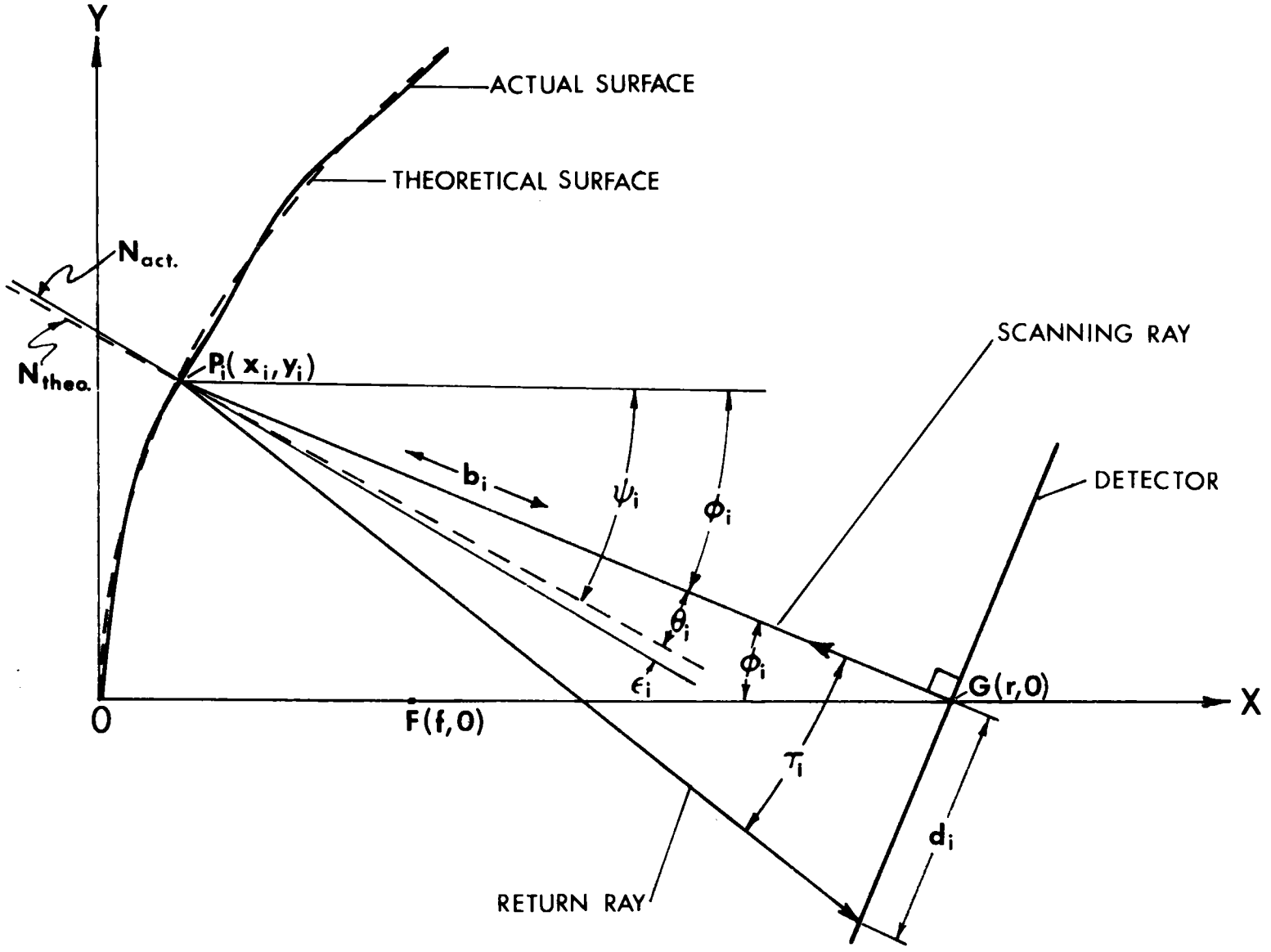

Figure 2. Radial Scan Laser Ray Trace Geometry

parabolic surface or, (2) apparatus set-up errors. These two types of deviations can be expressed in terms of either actual or apparent surface slope errors, respectively. Thus the positional and alignment errors must be minimized or accounted for systematically by data reduction to allow the surface contour and best fit focal point to be accurately determined. Surface slope errors may arise from either random imperfections and ripples, or systematic focal length errors. Set-up errors always introduce systematic slope errors.

Figure 3 shows the laser beam orientation after introducing positional and alignment errors x', y', and ϕ'. The two positional errors shift the pivot point to G'. The alignment error incorrectly indexes the angle of the scanning ray. With these errors the beam now intersects the collector at P_i' and the reflected ray intersects the detector a new distance d_i' from the center of the detector. The effect of these errors will be interpreted as an apparent slope error. Such effects on slope error measurement accuracy may be evaluated in terms of set-up tolerances. These tolerances must be achieved to insure sufficient accuracy in measuring the surfaces of parabolic mirrors having slope error distributions with standard deviations as small as 2 to 5 mrad (0.115 to 0.29 deg), and best fit focal length deviations on the order of ±2.5 mm (0.1 in).

GEOMETRIC RELATIONSHIPS AND ERROR SIMULATION

The idealized scanning geometry relates slope error ε_i measurements to four known or measured parameters: detector position d_i, scanning angle ϕ_i, scanning position r, and parabola focal length f. Equations relating these parameters can be adapted to simulate effects on slope error measurement and thus assess the sensitivity to errors in these parameters.

From Figure 2, the equations relating slope error to the measured parameters in the idealized situation are developed first.

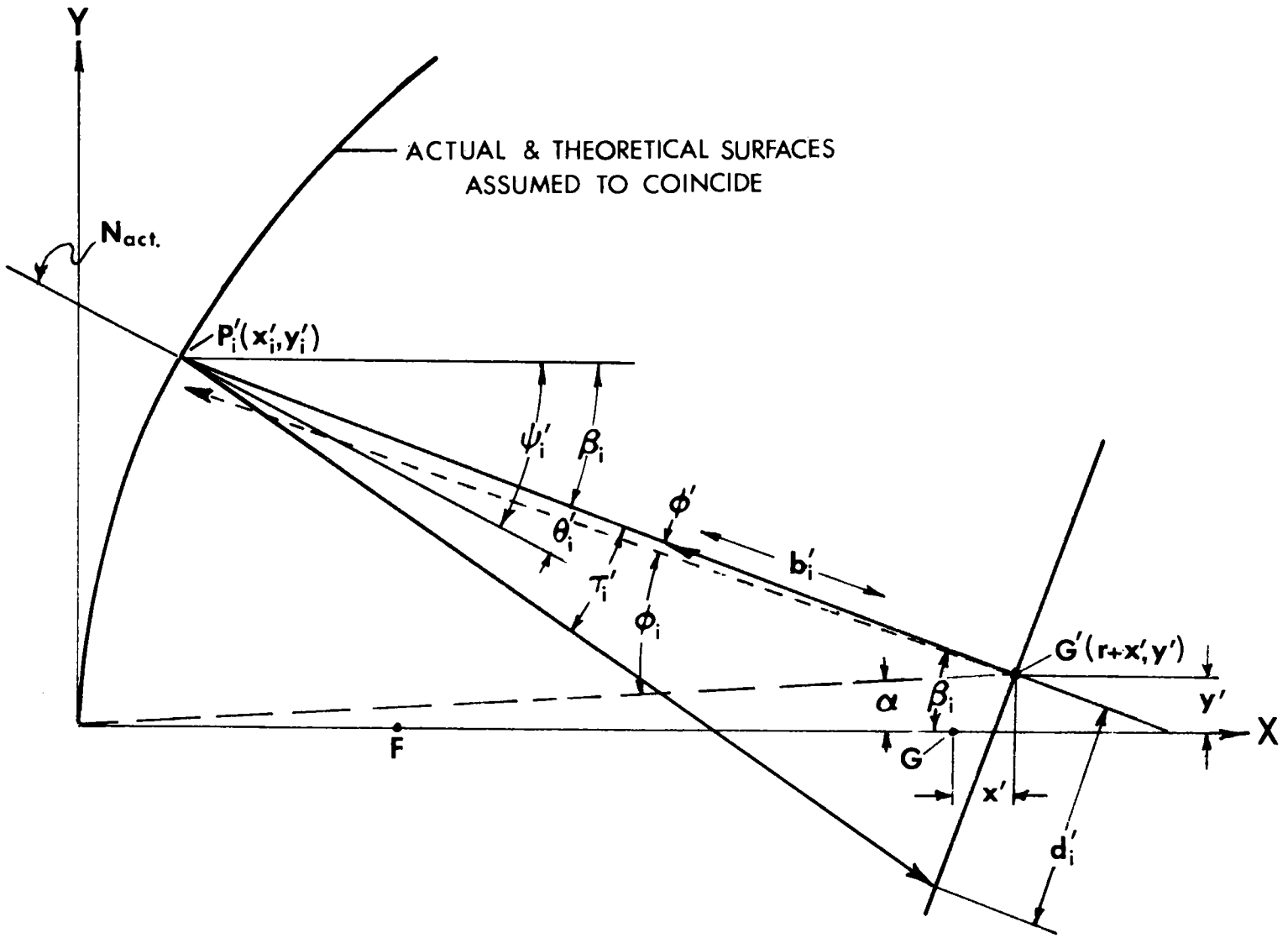

Figure 3. Effect of Set-Up Errors

STEP 1. The coordinates of P_i are determined from ϕ_i, r, and f.

$$\tan \phi_i = \frac{y_i}{r - x_i}$$

For a parabolic surface $x_i = \frac{y_i^2}{4f}$. Substituting for x_i the above equation becomes

$$\tan \phi_i = \frac{y_i}{r - \frac{y_i^2}{4f}}$$

Rearranging and simplifying

$$y_i^2 + \left(\frac{4f}{\tan \phi_i}\right) \cdot y_i - 4fr = 0$$

The roots of this quadratic are

$$y_i = -\frac{2f}{\tan \phi_i} \pm 2\sqrt{\left(\frac{f}{\tan \phi_i}\right)^2 + fr} \qquad (1)$$

where the sign of the radical is positive when ϕ_i is positive or clockwise with respect to the focal plane.

STEP 2. θ_i, the angle formed between the incident ray and the normal to the perfect parabolic surface at P_i is next determined.

$$\theta_i = \Psi_i - \phi_i$$

Now

$$\tan \Psi_i = \left.\frac{dx}{dy}\right|_{P_i} = \frac{y_i}{2f}$$

Therefore,

$$\boxed{\theta_i = \tan^{-1}\left(\frac{y_i}{2f}\right) - \phi_i} \qquad (2)$$

where y_i is given by equation (1).

STEP 3. In order to relate θ_i and ε_i (the slope error at P_i) to the position d_i of the return ray on the detector b_i (the distance between G and P_i), must first be calculated. This length is equal to

$$\boxed{b_i = \sqrt{\left(y_i - 0\right)^2 + \left(r - x_i\right)^2}} \qquad (3)$$

Now d_i depends on θ_i, ε_i, and b_i in that

$$\tan \tau_i = \tan\left(2\theta_i + 2(-\varepsilon_i)\right) = \frac{d_i}{b_i} \qquad (4)$$

The sign convention for ε_i chosen is such that a negative slope angle is always counter-clockwise with respect to the ideal parabola tangent. Using the relationship

$$\tan\left(2\theta_i - 2\varepsilon_i\right) = \frac{\tan 2\theta_i - \tan 2\varepsilon_i}{1 + \tan 2\theta_i \tan 2\varepsilon_i}$$

and substituting this into equation (4) and rearranging

$$\varepsilon_i = \frac{1}{2} \tan^{-1}\left(\frac{b_i \tan 2\theta_i - d_i}{b_i + d_i \tan 2\theta_i}\right) \tag{5}$$

In the case of a parabola with no slope errors, d_i will equal the quantity $b_i \tan 2\theta_i$ so that equation (5) goes to zero.

Using equations (1), (2), (3) and (5), a slope error at any point on the collector surface may be measured if the parabola focal length f, the scanning position r, the scanning angle ϕ_i, and the return ray position at the detector d_i, are all accurately known.

* * *

Equation (5) can also be used to calculate the <u>apparent</u> slope error ε_i' caused by set-up errors. To accomplish this equations (1), (2), (3) and (4) must be generalized to allow the prediction of the now displaced return point on the detector. This value, d_i', is then simply substituted for d_i in equation (5).

Referring to Figure 3 the generalized equations incorporating the positional and alignment errors are derived as follows:

$$y_i' = \frac{-2f}{\tan \beta_i} \pm 2\sqrt{\left(\frac{f}{\tan \beta_i}\right)^2 + f\left(r + x' + \frac{y'}{\tan \beta_i}\right)} \tag{1'}$$

where $\beta_i = \phi_i + \phi_i' - \alpha$ and $\alpha = \tan^{-1}\left(\frac{y'}{r + x'}\right)$

$$\boxed{\theta_i' = \tan^{-1}\left(\frac{y_i'}{2f}\right) - \beta_i} \qquad (2')$$

$$\boxed{b_i' = \overline{G'P_i'} = \sqrt{(y_i' - y')^2 + \left((r + x') - x_i'\right)^2}} \qquad (3')$$

$$\tan \tau_i = \tan 2\theta_i' = \frac{d_i'}{b_i'} \text{ or } \boxed{d_i' = b_i' \tan 2\theta_i'} \qquad (4')$$

In all of these equations it is now assumed that there are no <u>actual</u> slope errors in the parabola measured. The new return ray position d_i' has now been determined as a function of the three original system parameters plus the three set-up errors. This quantity may now be substituted for d_i in equation (5). Thus the <u>apparent</u> slope error is given as

$$\boxed{\varepsilon_i' = \frac{1}{2} \tan^{-1}\left(\frac{b_i \tan 2\theta_i - d_i'}{b_i + d_i' \tan 2\theta_i}\right)} \qquad (5')$$

From equation (5'), one can compute the apparent slope error on a theoretically perfect surface resulting from set-up errors x', y' and ϕ'. For the case of a perfectly positioned and aligned apparatus ($x' = y' = \phi' = 0$), d_i' will equal d_i

and $\varepsilon_i' = 0$. It should also be pointed out that the effects of an error in the assumed focal length can be evaluated by further generalization of the above equations. This is done by substituting $(f + f')$ for f in equations (1′) and (2′).

SIMULATION PROCEDURE

Using the above relationships apparent slope error patterns can be predicted or calculated for various combinations and magnitudes of apparatus set-up errors. A series of computer studies generating slope error patterns of ε_i' vs ϕ_i was implemented according to the plan shown in the matrix below.

	Computer Runs				
Error Type	a	b	c	d	e
X'	0	1	0	0	0
Y'	0	0	1	0	0
ϕ'	0	0	0	1	0
f'	0	0	0	0	1

In this matrix a "1" indicates that the respective variable was changed through a range of values to determine the sensitivity of the ε_i' vs ϕ_i plots to that respective set-up variable. A "0" indicates the variable was held equal to zero. Slope error patterns arising from focal length errors were also generated for purposes of comparison to the patterns due to set-up errors. In essence these patterns are finite difference approximations to the quantities $\frac{\partial \varepsilon'}{\partial \xi}$ plotted as functions of ϕ where ξ is any one of the set-up errors (x', y', or ϕ') or a focal length error f'.

The simulation results presented below are for scans of a typical practical parabolic shape with f = 0.658 m (25.9 in) and rim-to-rim aperature distance of

2.743 m (9 ft). This parabola is scanned from a scanning radius r of 1.817 m (71.5 in). In principle r can be chosen arbitrarily, but this optimum length minimizes the length and cost of the return beam detector. Scans made from smaller or greater radii respectively increase either the maximum return beam excursion in one direction at scanning angles of ±20°, or the excursion in the opposite direction when ϕ is at its maximum value of ±55°.

RESULTS AND DISCUSSION

General Slope Error Effects

The figures below demonstrate four distinct slope error patterns. The pivot position errors x' and y' are shown in Figures 4 and 5 respectively. An x' error produces a sine-like wave with maxima occurring where the scanning angle is approximately ±28°. Furthermore, these slope error patterns essentially scale proportionally with the magnitude of x'. Thus values for $\left.\frac{\partial \varepsilon'}{\partial x'}\right|_{\phi_i=k}$ are essentially constant over the range of values for x' investigated. Patterns generated by x' errors of 2.54, 5.08, and 12.7 mm (0.1, 0.2, and 0.5 in) are shown in this figure.

In Figure 5 patterns due to y' errors of 2.54, 5.08 and 7.62 mm (0.1, 0.2, and 0.3 in.) show a nominally constant shift of negative slope error throughout the scan. Once again $\left.\frac{\partial \varepsilon'}{\partial y'}\right|_{\phi_i=k}$ is constant.

Typical error patterns generated by angular alignment errors in the scanning angle are shown in Figure 6. The hat-like form of these curves becomes proportionally more pronounced as the size of ϕ' increases while the point of zero apparent slope error occurs always at a scanning angle of approximately 20°. These results indicate that apparent slope errors greater than 2 mrad (.115°) will be introduced if the scanning angle can not be accurately measured

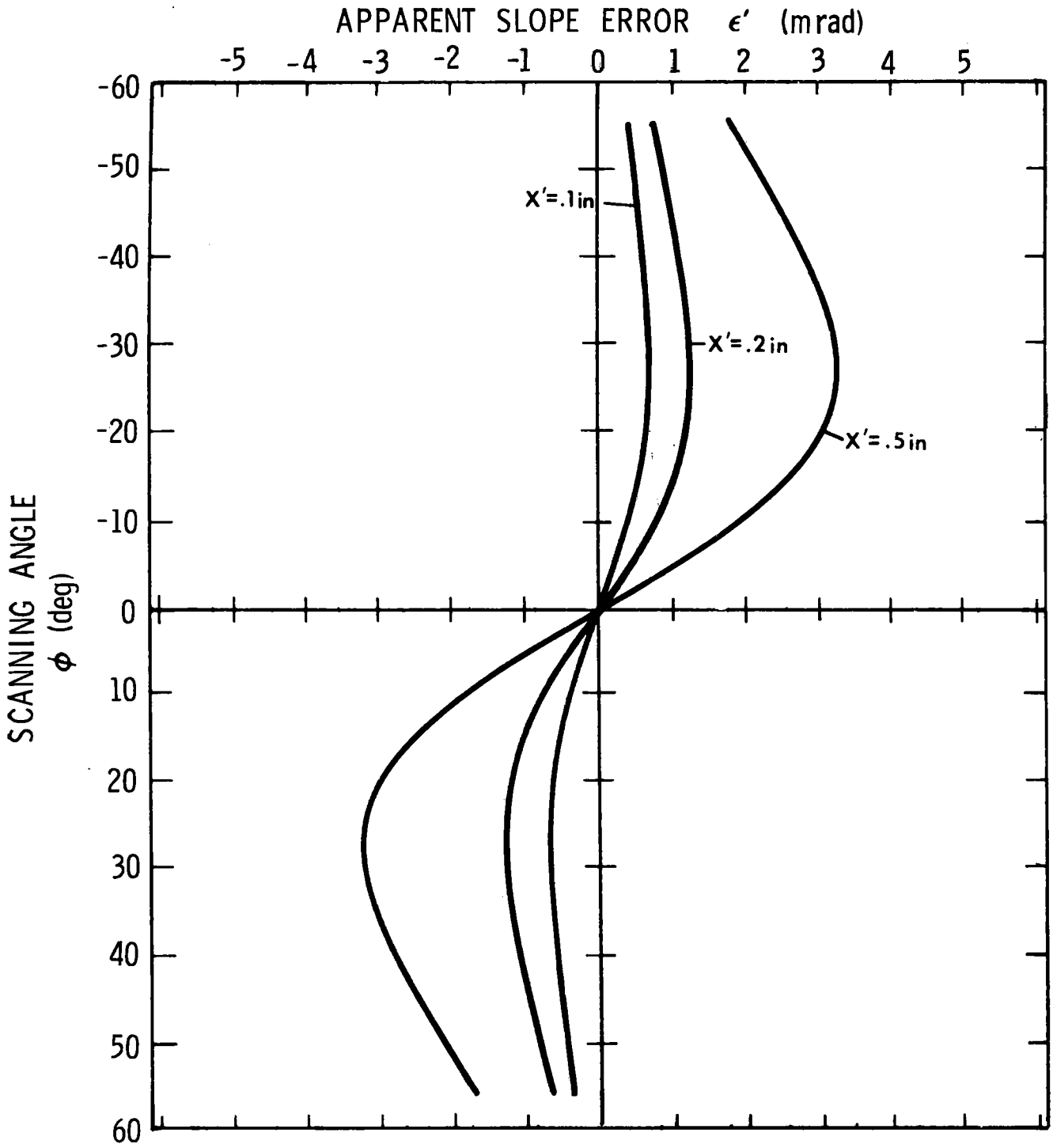

Figure 4. Slope Errors Induced by Positional Errors Within the Focal Plane

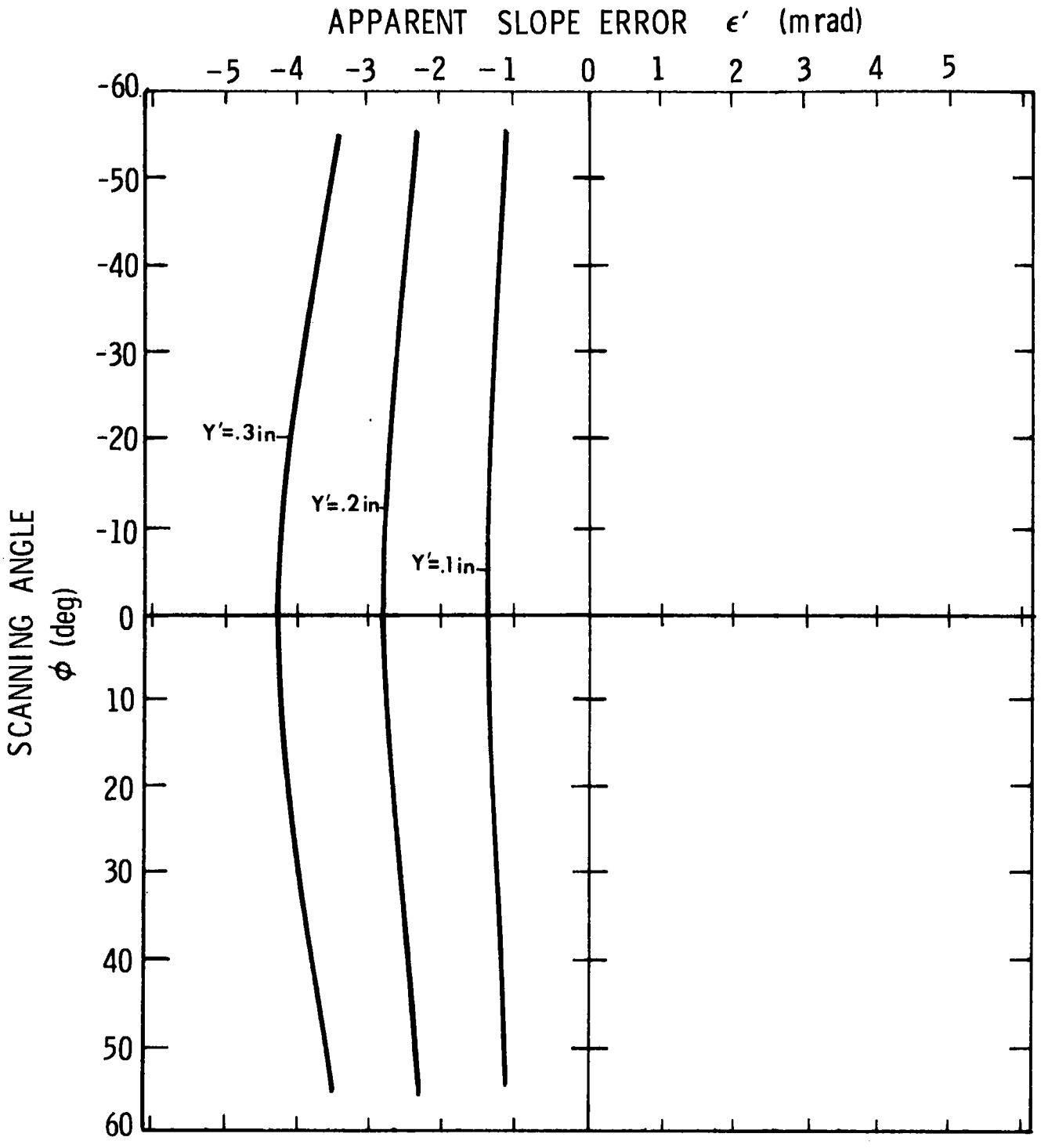

Figure 5. Slope Errors Induced by Positional Errors Away From Focal Plane

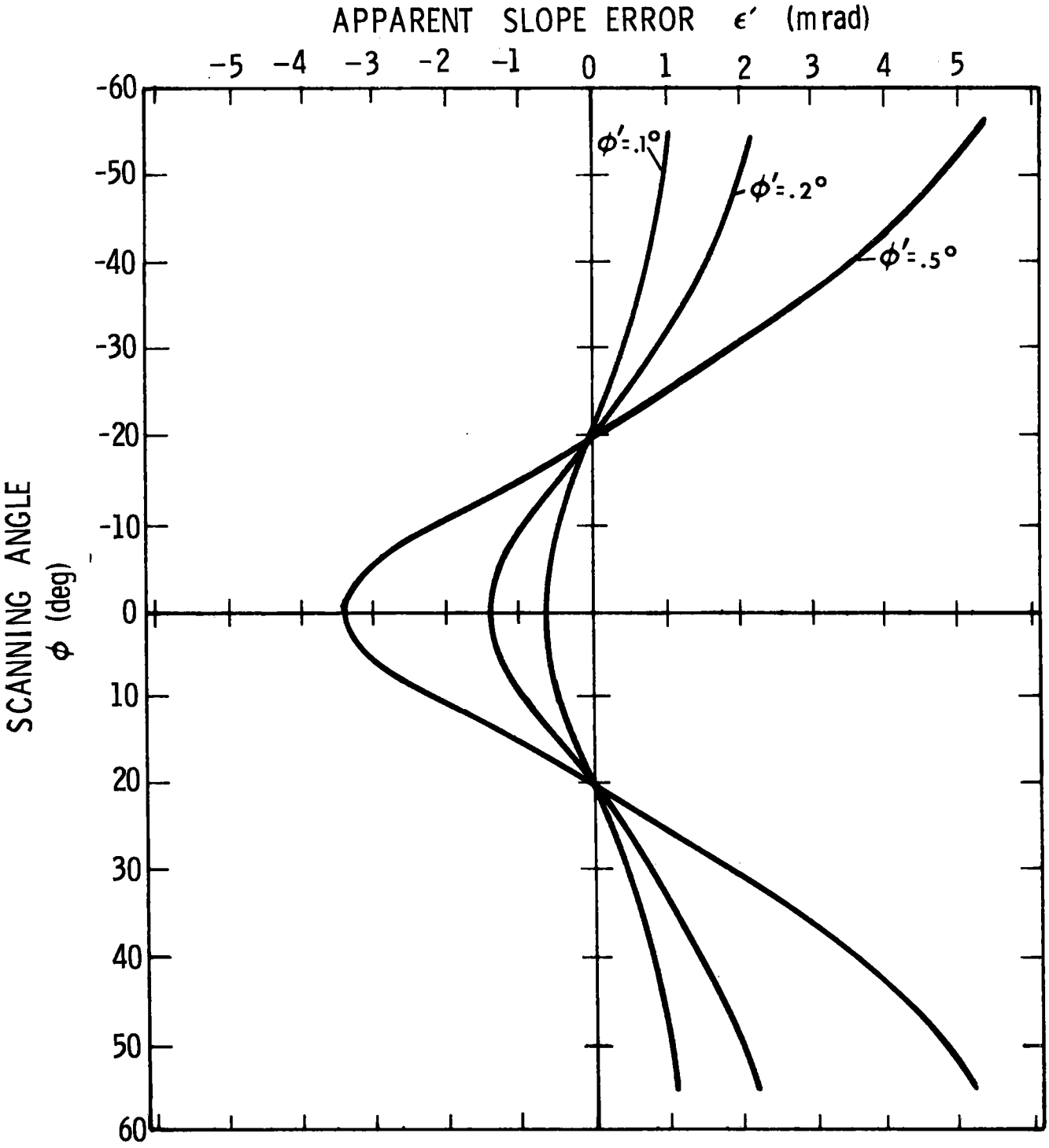

Figure 6. Slope Errors Induced by Indexing Errors in Scanning Angle or "Alignment Errors"

within ±4.36 mrad (0.25°) or better. Error patterns generated by ϕ' scale proportionally with the magnitude of ϕ'.

Finally, the patterns shown in Figure 7 predict the effects on the slope error measurement of mirrors having slightly longer focal lengths than expected while assuming all alignment parameters are accurately measured. These patterns are somewhat similar to the patterns generated by x' alignment errors for scanning angles in the -25° to +25° range. However, instead of reaching a maximum and then falling off again towards zero, these curves remain practically constant after reaching their maxima. The equal spacing between maxima of the three curves (-1.51, -3.01, and -4.51 mrad) demonstrates that values of $\left.\frac{\partial \varepsilon'}{\partial f'}\right|_{\phi_i=k}$ also remain constant.

Tolerance Implications

The distinct forms of the slope error patterns generated by y' and ϕ' errors offer the possibility for pattern recognition and subsequent correction of even small such errors by using appropriate curve unfolding techniques. However, this approach does not lend itself to distinguishing between the horizontal position error x' and a focal length error. This is especially true where these errors are small and the slope error curves are quite similar. However, in this case a simple proportional comparison between the respective error patterns should suffice to establish the positional tolerance. Thus for magnitudes of x' less than 15 mm (0.6 in), a constant ratio exists between f' and x' in terms of both standard deviations and maxima of their respective apparent slope error curves. A focal length error generates an apparent slope error curve with the same maximum as the respective curve due to an x' error approximately 2.36 times as great, or $\left.\frac{\partial \varepsilon'}{\partial x'}\right|_{\phi_i=k} = -2.36 \cdot \left.\frac{\partial \varepsilon'}{\partial f'}\right|_{\phi_i=k}$ for $-25° \leq \phi_i \leq +25°$. Assuming focal lengths must be determined within an accuracy of ±2.5 mm (.1 in.), the implied

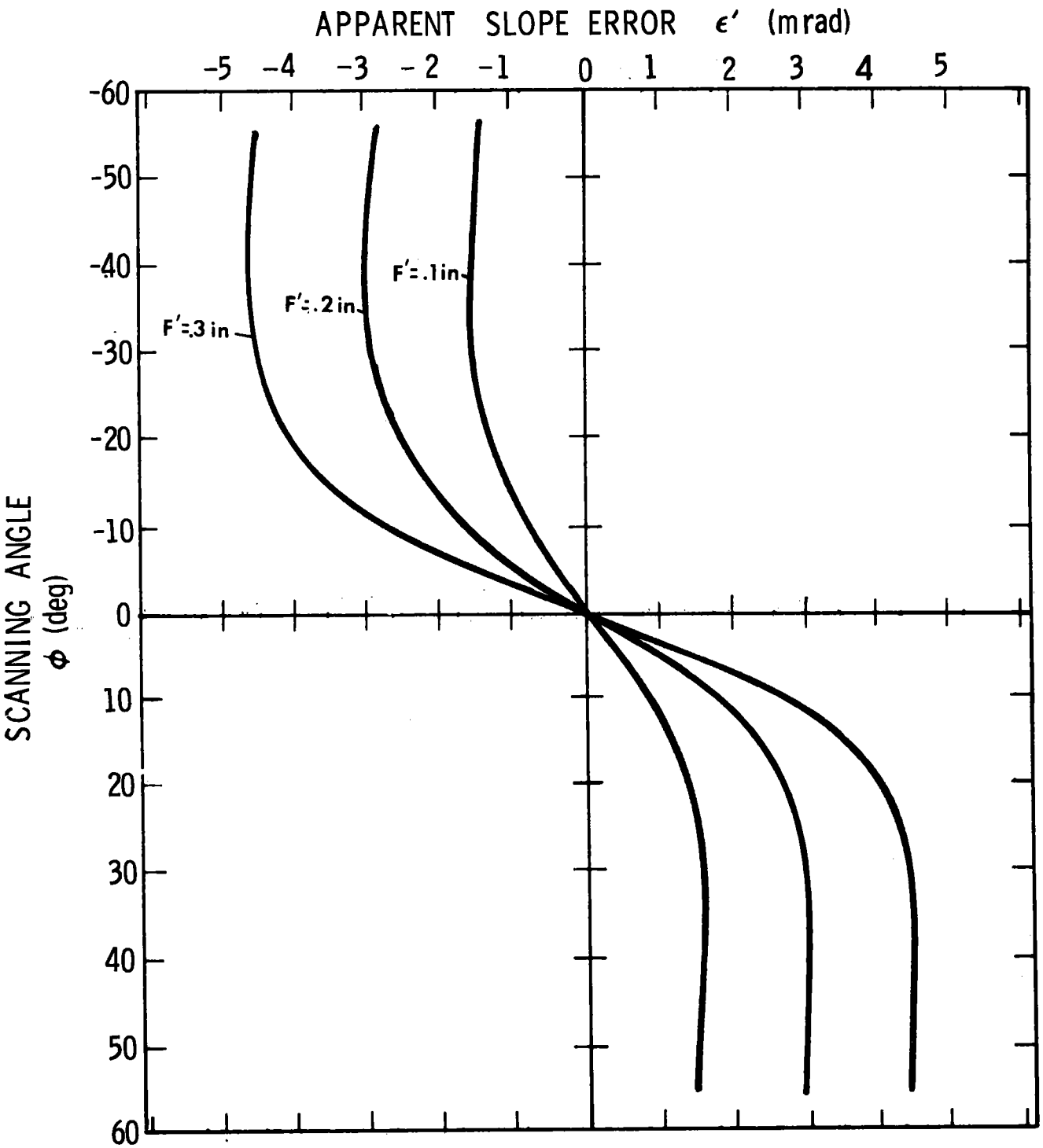

Figure 7. Slope Errors Induced by Focal Length Errors

tolerance for locating the scanning point within the focal plane would be ±5.9 mm (0.25 in.). Conversely, if x′ can be held within ±1 mm (.039 in.) then the accuracy of f for the best fit parabola calculated from a slope error distribution will be ±0.42 mm (0.017 in.). Although the supporting data are not given here, it can be shown that the accuracies of f measurements for all mirrors in the focal length range of 0.470 to 0.762 m (18.5 to 30 in.) are nominally 0.42 (1/2.4) times the x′ uncertainty.

Set Up Tolerance and Detector Resolution

The relevance of the above level of tolerance to measurement accuracy must be evaluated in terms of another constraint not yet discussed, i.e., the smallest detectable slope error, which is dependent on the detector resolution. Thus detector resolution determines the degree of inaccuracy with which the apparatus can be positioned and aligned before introducing detectable apparent slope errors. The most conservative criterion would be detection of the maximum apparent slope error in any pattern.

The detector used in the current system is made up of 360 discrete photo diodes mounted on 2.54 mm (0.1 mm) centers. It can resolve slope errors on the order of ±0.32 to ±0.54 mrad (0.019 to 0.031 deg) depending on the distance the detector is located from the surface being inspected. This distance varies from 1.17 to 1.93 m (46 to 76 in.) depending on the dimensions of the mirror to be measured, and to a lesser extent, on the scanning angle ϕ_1. For the 0.658 m (25.9 in.) focal length mirror discussed in this paper, this distance is assumed to be the optimal 1.82 m (71.5 in.) scanning radius, less the 12.7 cm (5 in.) detector arm. For such an arrangement the detector resolution is on the order of ±0.38 mrad (0.022 deg). (See Appendix for details.) Since an x′ error of ±1.51 mm (0.059 in.) can be expected to introduce a maximum* slope error of

*The threshhold value of x′ is exceeded by 50% before more than half the resulting slope error curve can be detected.

±0.38 mrad, location of the scanning point G with any greater accuracy would be superfluous. Using the same reasoning, it can also be shown that no focal length errors smaller than ±0.65 mm (0.026 in.) can be detected. These lower limits remain essentially the same for the entire range of mirror focal lengths and optimum scanning radii.

Extrapolation from Figures 5 and 6 for an effective detector resolution of ±0.38 mrad indicates that slope errors due to y' errors as small as 0.5 mm (0.02 in.) and ϕ' errors on the order of 0.032 deg (0.56 mrad) can be detected.*

Combined Set-Up Errors

An additional aspect of the measurement sensitivity to the three apparatus positioning and alignment errors has yet to be carefully examined. This concerns the effects of combining two or more errors. The possibilities include effects of both adding and subtracting apparent slope errors in a variety of combinations and relative magnitudes resulting in the creation of slope error patterns of varying complexity and magnitude. It may be that curve fitting and unfolding techniques can again adequately unravel such composite curves to permit data correction or compensation. Further study and analysis in this area is recommended. However, it can be shown from the data already generated that x', y', and ϕ' errors of +1.5 mm, -0.5 mm, and +0.032 deg respectively -- which individually are undetectable -- combine to generate a slope error pattern thirty percent of which will be seen by the detector.

CONCLUSIONS

1. Computer simulation of measurement errors due to positional and alignment uncertainties of the radial scan laser inspection system indicates

*It is again noted that ϕ' must be more than 0.06 deg before 50% of the resulting error curve is detected.

distinct patterns of systematic errors. Two types of these patterns -- those due to y' and ϕ' errors -- can be uniquely recognized and probably compensated using curve fitting and unfolding techniques.

2. The extent to which apparent slope error patterns due to x' positional errors resemble those introduced by focal length inaccuracy indicates that adequate compensation techniques may not be achievable. For this reason a factor on the order of 0.42 times the scanning radius uncertainty gives the error with which the best fit focal length can be estimated from a particular laser scan.
3. The detector resolution in effect establishes lower bounds on the practical tolerances required for all three set-up errors when considered individually. However, in the worst case combination the three kinds of slope error patterns add and thereby imply a requisite for yet closer tolerances.

REFERENCES

1. Discussion of an earlier version of this scanning system is presented in: B. L. Butler and R. B. Pettit, "Optical Evaluation Techniques for Reflecting Solar Concentrators," SPIE Vol. 114 Optics Applied to Solar Energy Conversion, 1977, pp. 43-49.
2. "Solar Total Energy Program Semiannual Report, October 1975-March 1976," SAND 74-0391, June 1976, pp. 51-54, available NTIS.

APPENDIX

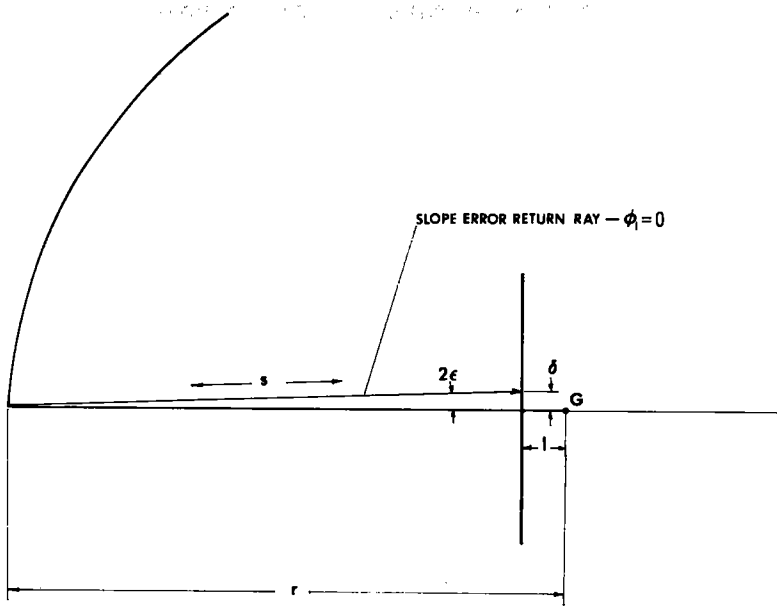

Figure A1. Calculation of slope error resolution.

The resolution of the detector in terms of slope error is a function of both the diode separation and the distance from mirror surface to the detector. Assuming the detector can discriminate between the case when a ray intersects two adjacent diodes simultaneously from the case when only one diode is intersected, the effective linear resolution δ of the detector itself is $\frac{0.1 \text{ in}}{2}$ or .05 in. (1.27 mm). Since the second parameter -- mirror to detector distance -- varies throughout the scan, only the worst case or smallest distance for each mirror type is considered in the calculations of slope error resolutions. In all three cases this distance was taken to be the optimum radius r minus ℓ (the 5 in. detector arm) when the scanning angle equals 0 deg. Thus slope error resolution = $\frac{1}{2} \tan^{-1} \frac{\delta}{r - \ell}$. Calculated values of slope error resolutions along with the values of f and r for three examples in the range of mirror designs considered are tabulated below.

f	r-ℓ	δ	Slope Error Resolutions (mrad)
cm (in)	cm (in)	cm (in)	mrad (deg)
47 (18.5)	116.8 (46)	.127 (.05)	±0.54 (.031)
65.8 (25.9)	168.9 (66.5)	.127 (.05)	±0.38 (.022)
76.2 (30.0)	193.0 (76)	.127 (.05)	±0.32 (.019)

Unlimited Release

Distribution:
TID-4500-R64, UC-62 (300)

Argonne National Laboratory
Attn: M. L. Kyle, Office of the Director
S. Zwerdling, Director of Solar Energy Programs
9700 South Cass Ave.
Argonne, Illinois 60439

Battelle Memorial Institute
Attn: K. Drumheller
Pacific Northwest Lab
P. O. Box 999
Richland, Washington 99352

U. S. Department of Energy
Solar Energy Division
Attn: G. M. Kaplan
S. Gronich
J. E. Rannels
M. U. Gutstein
20 Massachusetts Ave.
Washington, DC 20545

Midwest Research Institute
Attn: J. O. Bradley
425 Volker Blvd.
Kansas City, Missouri 64110

Jet Propulsion Lab
Bldg. 277, Room 201
Attn: V. C. Truscello
4800 Oak Grove Drive
Pasadena, California 91103

Ratheon, Inc.
Missile System Division
Attn: L. Paradis
Spencer Lab
Wayside Avenue
Burlington, Massachusetts 01803

Gus Hutchison
Solar Kinetics, Inc.
147 Parkhouse Street
P. O. Box 10764
Dallas, Texas 75207

Del Manufacturing Co.
905 Monterey Pass Road
Attn: M. M. Delgado
Monterey Park, California 91754

Dr. Barry L. Butler
Solar Energy Research Institute
1536 Cole Blvd.
Golden, Colorado 80407

Richard Waterman
Solar Intel
P. O. Box 38
Riverton, Connecticut 06065

B. P. Gupta
MN 17-T540
Honeywell, Inc.
2600 Ridgeway Parkway
Minneapolis, Minnesota 55413

Dr. Renato Bautista
Ames Lab
Iowa State University
Ames, Iowa 50011

Richard A. Farran, Manager
Thermal Systems & Cryogenics Section
The Aerospace Corp.
2350 E. El Segundo Blvd.
El Segundo, California

Cedric Currin
Energy Technology Manager
Dow Corning Corp.
Midland, Michigan 48640

John M. Caudle
Mail Station FA32
Marshall Space Flight Center
Huntsville, Alabama 35812

McDonnell-Douglas Astronautics
Attn: Dennis Krause
Richard Lamoureux
5301 Bolsa Avenue
Huntington Beach, CA 92647

Distribution (con't):

Glen E. McDonald
Bldg. 51
NASA, Lewis Research Center
Cleveland, Ohio 44135

Miss Mildred Post
National Bureau of Standards
Bldg. 226, Rm B348
Washington, DC 20234

Dr. David Soule
Dept. of Physics
Western Illinois University
Macomb, Illinois 61455

Steve Zender
G. T. Sheldahl
Northfield, Minnesota 55057

Tom Reitter
Mail Stop L302
Lawrence Livermore Lab
Livermore, California

Dr. John Venables
Martin Marietta Labs
Baltimore, Maryland 21227

Mr. John Blacklaw
FMC Corporation
Engineered Systems Div.
328 Brokaw Rd.
Santa Clara, California 95052

Lee D. LaGrange
General Atomic Co., Rm L512
P. O. Box 81608
San Diego, California 92138

Stan Moore
Los Alamos Scientific Lab
Los Alamos, New Mexico 87545

Dr. John Shepherd
University of Wisconsin - Riverfalls
Physics Department
Riverfalls, Wisconsin 54022

Dr. Keith D. Masterson
Solar Energy Research Inst.
1536 Cole Blvd.
Golden, Colorado 80401

1262 H. C. Hardee
Attn: C. E. Hickox
A. C. Ratzel
5231 F. Biggs
5710 G. E. Brandvold
5711 J. F. Banas
5712 J. A. Leonard
5712 G. W. Treadwell
5712 T. D. Harrison
5712 R. L. Champion
5713 W. Marshall
5714 R. P. Stromberg
5715 R. H. Braasch
5719 D. G. Schueler
5800 R. S. Claassen
Attn: 5810 R. G. Kepler
5820 R. L. Schwoebel
5830 M. J. Davis
5834 D. M. Mattox
Attn: R. R. Sowell
5840 H. J. Saxton
Attn: 5842 J. N. Sweet
5845 R. J. Eagan
5846 E. K. Beauchamp
5842 R. P. Pettit
5844 F. P. Gerstle, Jr. (3)
5844 L. Orear, Jr. (20)
8121 W. R. Delameter
8130 R. C. Wayne
8131 J. J. Bartel
8131 T. D. Brumleve
8131 W. G. Wilson
8132 A. C. Skinrood
8310 D. M. Schuster
8424 H. R. Sheppard
9352 O. J. Burchett
Attn: J. C. Bushnell
9352 B. D. Hansche
9572 L. G. Rainhart

3141 Technical Library (5)
3151 Technical Pub. (3) for DOE/TIC
(Public Release)
8266 E. A. Aas (1)